NUMERICAL ANALYSIS OF THE DIFFERENCES IN DIFFUSION BETWEEN *p*-SURFACE AND σ-SURFACE①

Yan Jinghua (阎敬华) and Xue Jishan (薛纪善)

Guangzhou Institute of Tropical and Oceanic Meteorology, Guangzhou, 510080

Received 9 December 1993, accepted 28 January 1995

ABSTRACT

Dimensional analysis and reduction are done to two existing schemes of 4th-order linear horizontal diffusion, and detailed control experiments between them are made using a topography-included mesoscale model. Horizontal diffusion is calculated on the σ-surface in one (known as Scheme A afterwards), and on the *p*-surface in another (Scheme B) . Experiments show that differences are small in smooth-terrain areas and very large in steep mountain areas, with the 24h rainfall prediction deviating by 50 mm between forecasts of the two schemes. The reason may be that temperature and humidity are falsely diffused in Scheme A, which causes abnormal temperature and humidity, and results in the anomalies of the unstable layer and convective processes. In addition, Scheme A could also bring about circulation anomalies which assumingly have direct link to the convective anomalies in the scheme. Furthermore, perturbation may also affect surrounding areas by wave-like propagation such that precipitation anomalies may occur in the area. The analysis indicate that Scheme B is necessary and feasible for it minimizes diffusion-involved forecast abnormality in steep mountains and areas around.

Key words: quasi-*p*-and σ-surface-based horizontal diffusion schemes, dimensional analysis, mesoscale model forecasts, control experiments

I. INTRODUCTION

Due to the turbulence in the atmosphere, the effect of non-linear diffusion needs to be in a numerical model. Dimensional analysis shows that parameterization of horizontal diffusion may be ignored, and diffusion terms may be replaced by resolvable horizontal advection and vertical mixing if resolution is $\leqslant$1 km horizontally and over 10 layers vertically (Taylor, 1954). It has to be considered otherwise. Among schemes commonly used for computing horizontal diffusion are of the 2nd (or 4th) order linear diffusion. A lot of attempts have been made in addressing the foregoing schemes and some problems arisen from the use of terrain-involved coordinates (e. g. σ-coordinates). Smargrinsky (1963) linked diffusion coefficients to velocity gradient and grid length. Meller et al. (1985) took the diffusion coefficients as zero when velocity reached zero so as to ac-

① This study is supported by the China's National Science Key Academic Program No. 85-906-03-07.

commodate diffusion of temperature and salinity in the area near steep orography. European Centre for Medium-Range Weather Forecast (1991) made them constant while calculating temperature diffusion on quasi-isobaric surfaces to suppress spurious warming near the mountain top, without treating moisture likewise. Based on characteristics of meso-scale models and a study by Smargrinsky (1963), Anthes et al. (1987) added a background value on to diffusion coefficients calculated on the σ-surface. It is proven in practice that it may bring about spurious diffusion for temperature and moisture, and thus lead to precipitation anomaly. Here , we use dimensional analysis and numerical experiments to further explore how linear diffusion schemes (e. g. Anthes et al. , 1987) calculated on the p-and σ-surfaces induce forecast differences so that mesoscale NWP can be improved in areas with steep topography.

Ⅱ. DESCRIPTION OF EXPERIMENTAL SCHEMES

The horizontal diffusion schemes for the comparative study are as below.

(a) For diffusion on the σ-surface (Scheme A), i. e. the one by Anthes et al. (1987), we define

$$F(\alpha) = \begin{cases} -K_{H4} \cdot \nabla_\sigma^4 & \text{for the inner area} \\ K_{H2} \cdot \nabla_\sigma^2 & \text{for the circle next to the lateral boundary} \end{cases} \tag{1}$$

where α could be any of the model variables, K_{H2} and K_{H4} are 2nd-and 4th-order horizontal diffusion coefficients respectively, which are defined as follows:

$$K_{H2} = A_{mp}\left(K_{H0} + \frac{1}{2}K^2 D \triangle S^2 \right) \tag{2}$$

$$K_{H4} = K_{H2} \triangle S^2 \tag{3}$$

where A_{mp} is lateral boundary amplification coefficient; K, Von-Carmon constant; K_{H0}, background value; D, deformation term proposed by Smargrinsky (1963).

(b) For diffusion on the p-surface (Scheme B), we define

$$F(\alpha) = \begin{cases} -K_{H4} \cdot \nabla_p^4 & \text{for the inner area} \\ K_{H2} \cdot \nabla_p^2 & \text{for the circle next to the lateral boundary} \end{cases} \tag{4}$$

where the symbols are all the same as in (1) . One may interpolate α vertically onto the corresponding p-surface to compute $F(\alpha)$ by (4). It needs much computation and yields large error. For simplicity, the classic transformation was done between σ-and p-coordinates . Ignoring greater than 2nd order partial differential terms of $\frac{\partial \alpha}{\partial \ln \sigma}$ with respect to x or y, we obtain

$$\nabla_p^4\alpha \doteq \nabla_\sigma^4\alpha - \frac{\partial\alpha}{\partial\ln\sigma}\nabla_\sigma^4(\ln\pi)$$

A B C

$$-4\frac{\partial}{\partial x}\left(\frac{\partial\alpha}{\partial\ln\sigma}\right)\left(\frac{\partial^3\ln\pi}{\partial x^3}\right)_\sigma - 4\frac{\partial}{\partial y}\left(\frac{\partial\alpha}{\partial\ln\sigma}\right)\left(\frac{\partial^3\ln\pi}{\partial y^3}\right)_\sigma$$

D

$$+\frac{\partial^2\alpha}{\partial\ln\sigma^2}\left[4\left(\frac{\partial\ln\pi}{\partial x}\right)_\sigma\left(\frac{\partial^3\ln\pi}{\partial x^3}\right)_\sigma + 4\left(\frac{\partial\ln\pi}{\partial y}\right)_\sigma\left(\frac{\partial^3\ln\pi}{\partial y^3}\right)_\sigma + 3\left(\frac{\partial^2\ln\pi}{\partial x^2}\right)_\sigma^2 + 3\left(\frac{\partial^2\ln\pi}{\partial y^2}\right)_\sigma^2\right] \tag{5}$$

E

It is easy to see that more simplification is needed for (5). Note that this mesoscale model is resolvable at 50 km (i. e. $\delta x \sim 5\times10^4$ m) in the horizontal, and 10 layers in the vertical (i. e. $\Delta Z \sim 10^3$ m), which reflects the meso-α scale perturbation. The order for (5) is assumed to be the value over maximally varied orography (e. g. around 1500 m per unit horizontal grid near Taiwan). The result from such dimensional analysis and simplification can be considered suitable for the whole model domain since the σ-coordinates is reduced to the p-coordinates in the area with smooth topography, so that the values for terms C, D, E in (5) approach zero. Based on the above analysis and mesoscale characteristics, the orders for some field variables may be given as below.

The horizontal variation scales for wind, temperature and moisture on isobaric surfaces over the δx scale are

$$\delta_p U \sim 10 \text{ m/s},\ \delta_p T \sim 10^0\text{—}10^1\ ^\circ\text{K},\ \delta_p Q \sim 10^{-3}\text{—}10^{-2}\ \text{g/g}$$

The corresponding scales on the σ-surface are

$$\delta_\sigma U \sim 10 \text{ m/s},\ \delta_\sigma T \sim 10^1\ ^\circ\text{K},\ \delta_\sigma Q \sim 10^{-2}\ \text{g/g},$$

in the vertical distance ΔZ ($\Delta\sigma \sim 0.1$) the scale for the above variables may be

$$\Delta U \sim 10^0 \text{ m/s},\ \Delta T \sim 10^1\ ^\circ\text{K},\ \Delta Q \sim 10^{-2}\ \text{g/g}$$

Now, the horizontal variation scales of the vertical changes for the above variables is

$$\delta\Delta U \sim \Delta U \sim 10^0 \text{ m/s},\ \delta\Delta T \sim 10^0\ ^\circ\text{K},\ \delta\Delta Q \sim 10^{-3}\ \text{g/g}$$

Since the partial differentiations with respect to x and y in (5) are simply a linear superposition and in completely the same form of expression but mutually independent, the two dimensional analysis can be represented by a one-dimensional case with respect to x. For simplicity, what is given below is one dimensional analysis with respect to x.

$$\frac{\partial^4\alpha}{\partial x^4} \doteq \alpha_{i+2} + 6\alpha_i - 4\alpha_{i-1} - 4\alpha_{i+1} + \alpha_{i-2}$$

$$= 3(\alpha_i - \alpha_{i-1}) + 3(\alpha_i - \alpha_{i+1}) + (\alpha_{i+2} - \alpha_{i+1}) + (\alpha_{i-2} - \alpha_{i-1}) \tag{6}$$

where the subscript i denotes the ith grid point in x direction, then

$$\left(\frac{\partial^4 u}{\partial x^4}\right)_p \sim \frac{1}{\delta x^4}\delta_p U \sim \frac{1}{\delta x^4}\times 10^1 \tag{7}$$

$$\left(\frac{\partial^4 u}{\partial x^4}\right)_\sigma \sim \frac{1}{\delta x^4}\delta_\sigma U \sim \frac{1}{\delta x^4} \times 10^1 \tag{8}$$

$$\left(\frac{\partial^4 T}{\partial x^4}\right)_p \sim \frac{1}{\delta x^4}\delta_p T \sim \frac{1}{\delta x^4} \times (10^0 - 10^1) \tag{9}$$

$$\left(\frac{\partial^4 T}{\partial x^4}\right)_\sigma \sim \frac{1}{\delta x^4} \times (1-6)\delta_\sigma T \sim \frac{1}{\delta x^4} \times (1-6) \times 10^1 \tag{10}$$

$$\left(\frac{\partial^4 q}{\partial x^4}\right)_p \sim \frac{1}{\delta x^4}\delta_p Q \sim \frac{1}{\delta x^4} \times (10^{-3} - 10^{-2}) \tag{11}$$

$$\left(\frac{\partial^4 q}{\partial x^4}\right)_p \sim \frac{1}{\delta x^4} \times (1-6) \times \delta_\sigma Q \sim \frac{1}{\delta x^4} \times (1-6) \times 10^{-2} \tag{12}$$

While $$\frac{\partial^4}{\partial x^4}(\ln\pi) \sim \frac{1}{\delta x^4} \times (1-6)\ln\left(\frac{700}{800}\right) \sim \frac{1}{\delta x^4} \times (1-6) \times 10^{-1} \tag{13}$$

we get

$$\frac{\partial u}{\partial \ln\sigma}\frac{\partial^4}{\partial x^4}(\ln\pi) \sim \frac{\Delta U}{\ln(0.85/0.95)} \times \frac{1}{\delta x^4} \times (1-6) \times 10^{-1}$$

$$\sim \frac{1}{\delta x^4} \times (1-6) \times 10^0 \tag{14}$$

$$\frac{\partial T}{\partial \ln\sigma}\frac{\partial^4}{\partial x^4}(\ln\pi) \sim \frac{1}{\delta x^4} \times (1-6) \times 10^1 \tag{15}$$

$$\frac{\partial q}{\partial \ln\sigma}\frac{\partial^4}{\partial x^4}(\ln\pi) \sim \frac{1}{\delta x^4} \times (1-6) \times 10^{-2} \tag{16}$$

In addition,

$$\frac{\partial^3(\ln\pi)}{\partial x^3} \sim \frac{1}{2\delta x^3}\left(\ln\frac{\pi_{i+2}}{2\pi_{i+1}} - \ln\frac{\pi_{i-2}}{2\pi_{i-1}}\right) \sim \frac{1}{\delta x^3} \times (10^{-1} - 10^{-2}) \tag{17}$$

$$\frac{\partial}{\partial x}\left(\frac{\partial u}{\partial \ln\sigma}\right) \sim \frac{1}{\delta x}\frac{1}{\delta \ln\sigma}(\delta\triangle U) \sim \frac{1}{\delta x} \times 10^1 \tag{18}$$

therefore,

$$4\frac{\partial}{\partial x}\left(\frac{\partial u}{\partial \ln\sigma}\right)\frac{\partial^3}{\partial x^3}(\ln\pi) \sim \frac{1}{\delta x^4}(10^{-1} - 10^0) \tag{19}$$

$$4\frac{\partial}{\partial x}\left(\frac{\partial T}{\partial \ln\sigma}\right)\frac{\partial^3}{\partial x^3}(\ln\pi) \sim \frac{1}{\delta x^4}(10^{-1} - 10^0) \tag{20}$$

$$4\frac{\partial}{\partial x}\left(\frac{\partial q}{\partial \ln\sigma}\right)\frac{\partial^3}{\partial x^3}(\ln\pi) \sim \frac{1}{\delta x^4}(10^{-3} - 10^{-4}) \tag{21}$$

Similarly the scales for E can be estimated in eq. (5). Note that the units of the variables and their derivatives from (7) to (21) were ignored because the same units (ISO system) were adopted in both sides of (5). From the dimensional analyses, we may be able to obtain a table showing the scales for each term in eq. (5).

Table 1 illustrates that in respect of winds terms A and B have the same order while terms C, D, E are more than half to one order smaller than term A. To save the amount

Table 1. Scales for each term in (5).

Elements	Terms				
	A	B	C	D	E
u, v	10^1	10^1	10^0-10^1	$10^{-1}-10^0$	$10^{-1}-10^0$
T	10^0-10^1	10^1-10^2	10^1-10^2	$10^{-1}-10^0$	$10^{-1}-10^0$
q	$10^{-3}-10^{-2}$	$10^{-2}-10^{-1}$	$10^{-2}-10^{-1}$	$10^{-4}-10^{-3}$	$10^{-4}-10^{-3}$

of computation, 0th order approximation may be assumed, i.e.

$$F(\alpha) \doteq - KH_4 \nabla_\sigma^4 \alpha \qquad (\alpha \sim u, v) \tag{22}$$

Numerical experiments showed that for variables u and v, the forecast difference between 0th and 1st order approximation is negligible. Therefore 0th approximation as in (22) is appropriate. For variables T and q, however, terms B and C have the same order while term A is about one order smaller than term B, and terms D and E are about one order further smaller than term A. This implies that term A is a small difference between the two large terms B and C, which cannot be neglected. On the other hand, as the 1st order approximation, terms D and E may be neglected. Thus we assume:

$$F(\alpha) \doteq - K_{H4}\left[\nabla_\sigma^4 \alpha - \frac{\partial \alpha}{\partial \ln \sigma} \nabla_\sigma^4 (\ln \pi)\right] \qquad (\alpha \sim T, q) \tag{23}$$

The numerical experiments described later show that eq. (23) is also suitable.

In the same way, for the grids next to the lateral boundary, it may be simplified as

$$F(\alpha) \doteq \begin{cases} - K_{H2} \nabla_\sigma^4 \alpha & (\alpha \sim u, v) \\ K_{H2}\left[\nabla_\sigma^4 \alpha - \dfrac{\partial \alpha}{\partial \ln \sigma} \nabla_\sigma^2 (\ln \pi)\right] & (\alpha \sim T, q) \end{cases} \tag{24}$$

Ⅲ. ANALYSES OF CONTROL NUMERICAL EXPERIMENTS

To compare the two diffusion schemes in a mesoscale model, a study on precipitation forecast was done. The case was Typhoon 8009 (Kim) that landed at Lufeng, Guangdong and dissipated (from 12Z, 27 July 1980 to 12Z, 28 July 1980) while moving northward. According to the *Typhoon Yearly Report* 1980 (1981), the typhoon brought about heavy precipitation in southern Guangdong, Dongsha Islands and southeastern Fujian but only minor rainfall over southeastern Taiwan coast. The initial model fields were obtained by interpolating the ECMWF analysis data on 5°× 5° grids on to the model's. Therefore the model outputed weaker intensity of typhoon and precipitation. For later convenience, the test on horizontal diffusion calculated on the σ-surface is noted as Experiment A, while that on p-surface as Experiment B.

Both experiments well predicted the recurvature variations of the circulation (Figure not shown). It is convinced that the model is capable of predicting the life cycle of the typhoon, and its results can be used for further analysis.

Scheme B is aimed to alleviate the deviations of model prediction in areas with steep orography, which normally occurs with Scheme A. Thus attention is on the model result for Taiwan. Fig. 1 is a contouring plot for the height of model orography around Taiwan. It is dominated by the Central Mountains stretching north-south in the east of Taiwan with maximum model height at 1643 m and steep slopes. In the mainland area, however, the model is generally covered with mild hills.

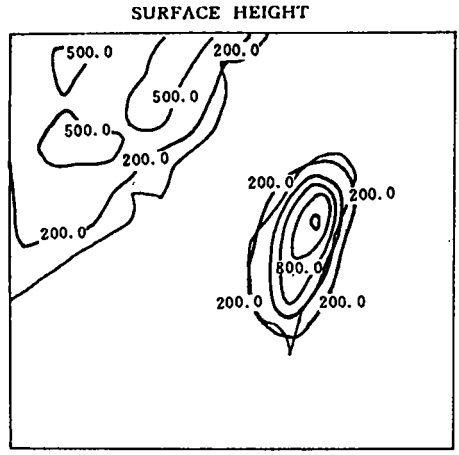

Fig. 1. Model terrain height around Taiwan Island. Thick solid line—coast, thin solid—contour (interval of 300 m)

Fig. 2a exhibited that the actual precipitation appeared in the southeastern

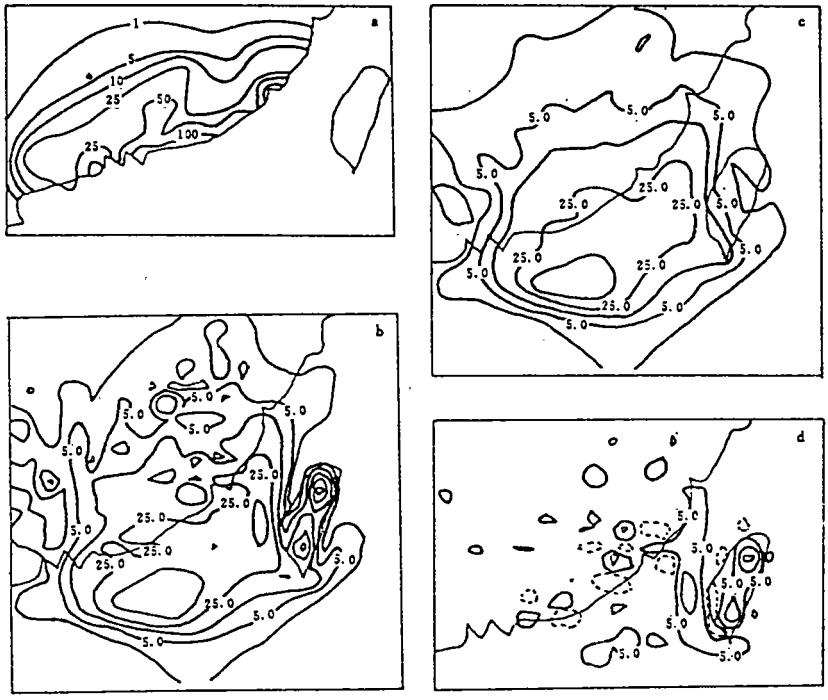

Fig. 2. Twenty-four hr rainfall from 12Z, 27 July, to 12Z, 28 July. a, observed; b, forecast of Scheme A; c, forecast of Scheme B; d, difference between b and c. (Contour values of 1, 5, 10, 25, 50, 100 mm for panels a, b, c, and ±5, ±20, ±50 mm for panel d; solid line—positive and dashed line—negative).

coast of Guangdong and Fujian. From the *Typhoon Yearly Report* 1980 (1981), there existed heavy rainfall in the Dongsha Islands (around 116. 7°E, 20. 8°N), but only a little precipitation was observed at some stations in southern Taiwan. It can then be judged that the actual precipitation was centred along the coast of Guangdong and Dongsha Islands while only nominal precipitation was recorded in Taiwan . In Experiment A (Fig. 2b), the precipitation is generally distributed in consistence with reality except for the Taiwan area, though the amount of predicted precipitation is much smaller than the actual value. It is worth noting that the model forecast produced two rainfall centres of over 50 mm in the northern and southern parts , where the steep orography exists (see Fig. 1). They did not exist in real case, and was resulted from inappropriate model representation of horizontal diffusion on the σ-surface. In addition, the model yielded many scattered precipitation centres in the mainland area due to orogràphic effect. In Experiment B (Fig. 2c) the overall scenario on the distribution and relative maxima of precipitation generally correspond to Experiment A. However, there was an obvious improvement, i. e. the false centres in Taiwan were removed and furthermore the contours of precipitation over the mainland area were smoother. The more real results in Experiment B implied that it performed better than Scheme A. Fig. 2d showed the difference of forecast precipitation. It showed that there were a number of centres , two of which were in the east of the island's northern and southern parts, with maximum value of more than 50 mm. Another two centres of precipitation difference were on the Taiwan Strait and Fujian, respectively, with maximum value over 20 mm. In addition, many more centres were found with absolute maxima above 5 mm. It suggested that the extent of forecast anomaly had close link with the slope of orography not only in areas of steep orography but also in the areas nearby (e. g. Taiwan Strait).

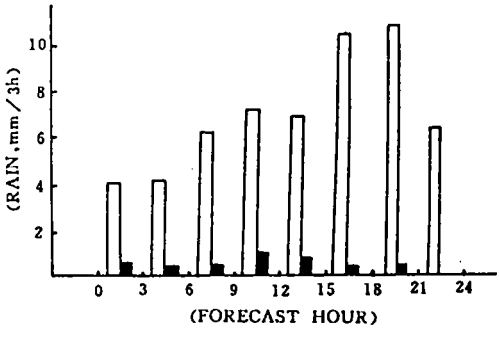

Fig. 3. Histogram of rainfall forecasts every 3 hours at (121. 4°E, 24. 4°N). Hollow column is for Scheme A, solid column for Scheme B.

Fig. 3 is a histogram which showed precipitation forecast every 3 hours over the centre point for northern Taiwan. It displayed that in the whole forecast period the accumulated precipitation by Scheme A for each of the three hour periods was more than 4 mm, and reached over 10 mm around the 18th hour (midday) . Furthermore, these precipitation processes were primarily convective. Obviously, the model forecast result by Scheme A can not be true in comparison with reality. Nevertheless, the accumu-

lated precipitation every three hours in Experiment B kept small, with the maximum value just about 1 mm. The above analysis denoted that in the whole forecast period the differences of 3-h precipitation forecast between the two schemes kept enormous, and Scheme A continuously produced considerable unrealistic precipitation.

To study the cause of the abnormal precipitation, variation of some elements with time at the point is given in Fig. 4. The ground temperature in Experiment A is higher than that in Experiment B by 0.5—2.0°K, and its difference between the two schemes is larger during the nighttime (0—12 h forecast) than during the daytime (12—24 h forecast). The trapezoidal line reflects the inclusion of radiative processes every 2 hours. The temperature at the lowest model level was also about 0.1—1.5 °C higher in Experiment A . Its difference was much smaller before mid-day (0—16 h) than after

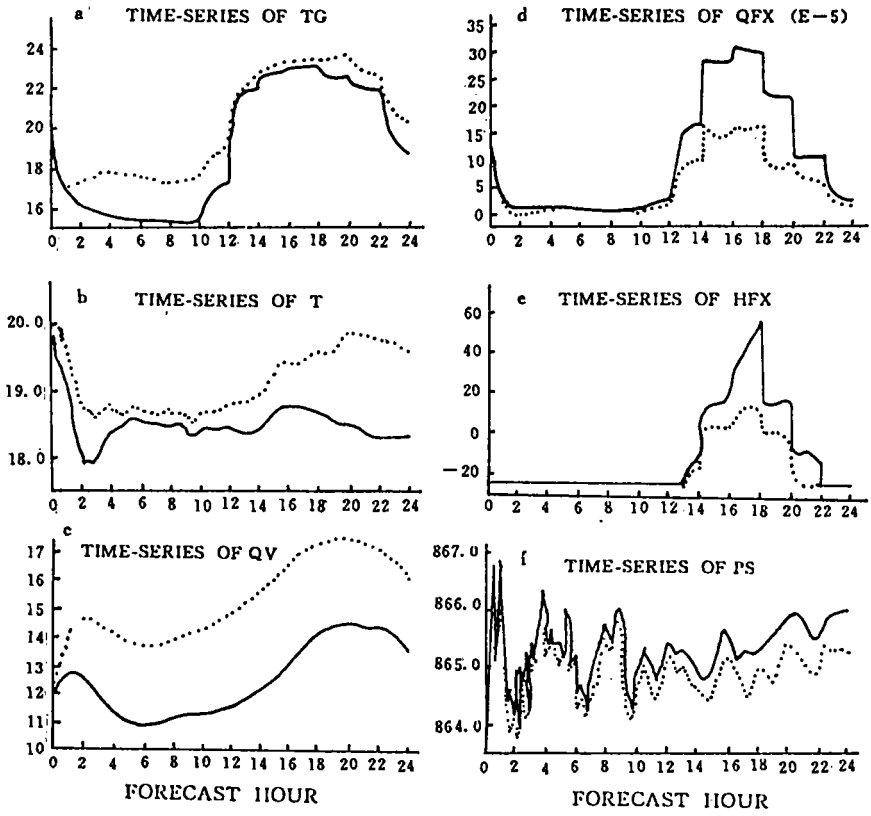

Fig. 4. Temporal variations of factors in the forecasts at point (121.4°E, 24.4°N). a. surface temperature (°C); b & c, temperature (°C) and specific humidity (g/kg) at lowest model level; d, e & f, vapor flux ($kg/m^{-2}s^{-1}$), sensible heat flux (Wm^{-2}) & pressure (hPa), at surface. Solid (dashed) line for Scheme A (B).

mid-day for 18—24 h (Fig. 4b). Furthermore, the specific humidity at the level was about 2.5 g/kg larger in Experiment A for the whole forecast period (Fig. 4c). They resulted in smaller moisture and sensible heating flux on the earth surface in Experiment A than in Experiment B (Fig. 4d,e). Therefore, in Experiment A the abnormally large precipitation at lower levels over the location was not due to strong fluxes of moisture and sensible heating but rather the "pumping-in" of surrounding high temperature and humidity due to the spurious diffusion on the σ-surface. In addition, the surface pressure in Experiment A was always lower than that in Experiment B, with the difference growing with time, and exceeding 0.7 hPa at 24 h. It well matches with the abnormally large precipitation in Experiment A. The foregoing analysis explained that Scheme A resulted in continuously unrealistic increase of surface temperature in mountain-top areas, temperature and specific humidity at the lowest model level, accompanied by continuously unrealistic decrease of surface sensible heating and moisture flux as well as surface pressure . However, the decrease of surface pressure and the increase of convection and precipitation were mutually complementary while the weakening of surface sensible heating flux and moisture was unfavourable for precipitation. It is thus necessary to further explore why the unrealistic increase of precipitation occurred in Experiment A.

To elucidate the occurrence of the anomalous precipitation in Experiment A, the time variation of the vertical structure of thermodynamic elements of interest is given in Fig. 5. The temperature at the lowest model level was always higher in Experiment A than in Experiment B, the difference increasing with time from 0.6°K at 6 hr to 2.5° K at 24 hr (Fig. 5a). It is understood from (6) that the temperature increase was caused by the false effect of horizontal diffusion on the σ-surface near the mountain top, which is in favour of the development of convective processes. Furthermore, the temperature around 370 hPa ($\sigma=0.35$) was also constantly higher in Experiment A with the difference having its maximum at mid-day (18 hr) , apparently due to active convective heating, which was the strongest around that level. The temperature difference at other levels appeared in irregular signs, which may be comprehensively caused by temperature rise, convective heating (upper layers) and horizontal diffusion (lower layers), and temperature drop by airmass uplifting as well as vertical propagation of wavetrain by anomalously forced perturbations, and so on, in Experiment A. The development of convective processes was indeed more active in Experiment A, particularly around mid-day (18 hr). It is consistent with the previous result. Meanwhile, due to the spurious horizontal diffusion on the σ-surface and strengthening of convective convergence, the specific humidity was always much higher in Experiment A than in Expriment B, particularly below 500 hPa, contributing to the increased convection in Experiment A. Fig. 5b exhibited that the Q_w value below 300 hPa was increasingly higher with the lowering of levels in Experiment A than in Experiment B due to the deviation of temperature and

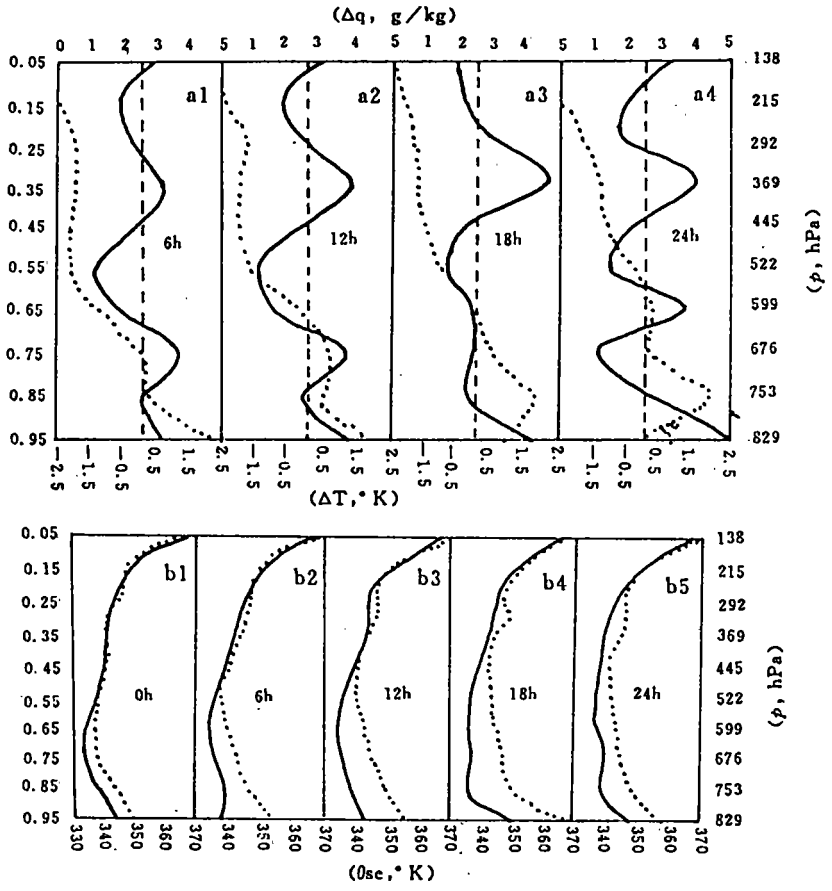

Fig. 5. Vertical distribution of factors for specified forecast hours. a, temperature & humidity deviations of Scheme A from Scheme B, with unit of °K & g/kg, at point (121.4°E, 24.4°N) b, Q_{se} (Soild lines denote Scheme B, and dotted Scheme A, but for Panel b1, solid line denotes analysis of 1200 GMT, July 27, dotted for that of 1200 GMT, July 28, unit: °K).

moisture produced by the effect of unrealistic diffusion on the σ surface (Fig. 5a). Furthermore, the conditionally unstable layer (i.e. the layer with $Q_{se}>p$) in Experiment A was much thicker, too, and reached 445 hPa at 18 hr while the conditionally unstable layer was weak and thin in Experiment B. Comparing Figs. 5b5 with 5b1, the analysed Q_{se} value at the lowest level was 348°K at 1200 GMT, 28 Jul., while the 24 hr forecast results from initial time 1200 GMT, 27 Jul., in Experiments A and B were 359°K and 348°K, respectively, i.e. the predicted Q_{se} profile in Experiment B corresponded well with the analysis whilst Experiment A incorrectly produced the Q_{se} value 11°K larger than the analysis and the thickness of the conditionally unstable layer much larger than reality. Just because of the spurious effect of horizontal diffusion on the σ-surface in Ex-

periment A, the model produced larger specific humidity at lower to middle levels near mountain top and higher temperature at lower model levels, leading to the thickening and strengthening of the unstable layer and overdevelopment of convective processes, and consequently the continuous and spurious increase of precipitation. Such phenomena were not present in Experiment B.

As known previously in Fig. 2d, Experiment A predicted anomalous precipitation in areas not only with steep slopes but with smooth surface (e. g. Taiwan Strait). It is thus necessary to analyse the anomalies of its whole horizontal field. Fig. 6 showed the forecast anomalous fields of temperature, specific humidity and wind vector (forecast difference between Experiments A and B) at 18 hr at the lowest model level. It is seen from the temperature anomalous field that there were two centres of +1 °K in eastern Taiwan, corresponding to the areas with steep 3-side orography in the northern and southern parts of the Central Mountains (Fig. 1). The pattern of the temperature anomalous field explained the unrealistic effect of the horizontal diffusion on the σ-surface and corresponded well with the two centres of positive precipitation anomaly as in Fig. 2d, and with the results as in Figs. 4 and 5. In the western coast of Taiwan, there existed two negative centres of temperature anomaly of 1°K, which were respectively in accordance with the two positive ones to the east and as a result of unrealistic effect of horizontal diffusion on the σ-surface.

Furthermore, the two negative anomalous centres of temperature corresponded to the ones of precipitation (Fig. 2d), denoting that the anomaly for the latter was resulted from the enhanced descent movement and weakened convective processes. In other areas, however, the temperature anomaly was small. It is seen that the unrealistic σ-surface diffusion effect on the rise (fall) of model temperature was very significant in the areas with steep mountain slopes, and otherwise in other areas. The difference field of specific humidity (Fig. 6c) was similar to that of temperature. The distribution of specific humidity confirmed the result that the anomaly of the model variable field was arisen from the spurious effect of the horizontal diffusion on the σ-surface, as already shown in Figs. 4 and 5. It is worth mentioning that the anomalous distribution of temperature was different vertically while that of specific humidity was generally homogeneous in mid-lower troposphere (Figure not shown). It corresponded to the result explained in Fig. 5a. Due to the coupling of anomalous distribution of specific humidity with temperature, an unrealistic anomalous circulation was formed in Experiment A, which led to the spurious precipitation anomaly as in Fig. 2d. The wind vector anomalous field (Fig. 6e) showed a significant convergence zone in the mountain area in eastern Taiwan, with the maximum vector length of 5 m/s. It corresponded to the areas with positive anomaly of temperature, moisture, precipitation, and conditional instability. Or, the horizontal diffusion on the σ-surface produced temperature and specific hu-

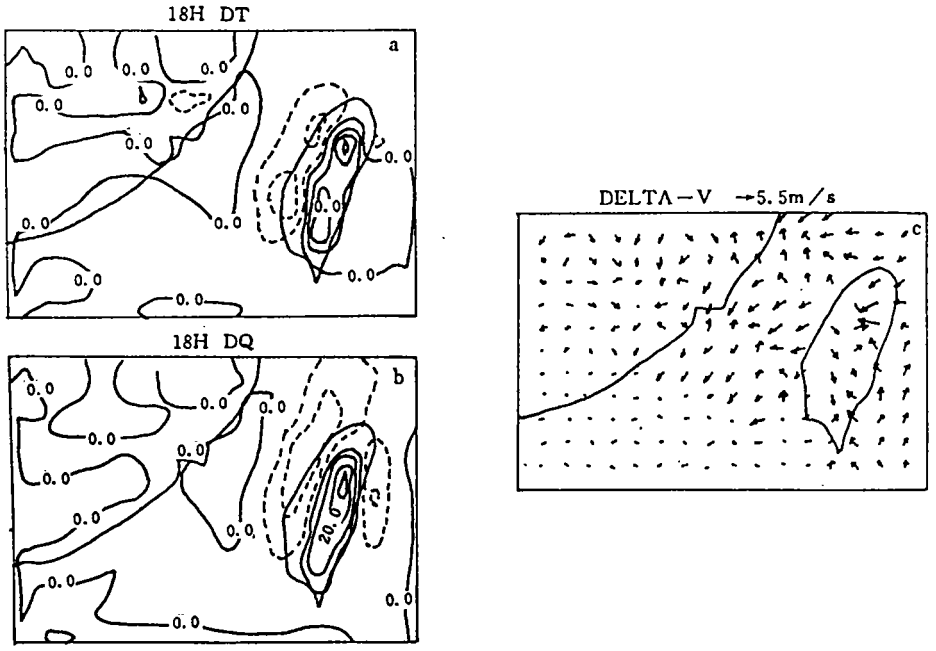

Fig. 6. Deviation fields (Scheme A minus Scheme B) at the lowest model level at the 18th forecast hour. a, temperature; b, specific humidity; c, wind. The solid line is for the positive value, the dashed negative, contour interval at 0.5°K & 0.5 g/kg, respectively.

midity anomalies so as to strengthen the low-layer convergence and convection near the mountain peaks. On the other hand, the divergence zone in the western coast of Taiwan corresponded to the area of negative anomaly of temperature, moisture and precipitation. It is worth noticing that there was a significant convergence zone of wind vector anomaly in central to southern Taiwan Strait. It signified active development of convective processes and corresponded well with the positive centre of precipitation anomaly in the strait. The convergent flow compensated for the divergent flow to the east. This compensatory flow may be taken as the result of westward propagation of perturbation in the form of internal gravity wavetrains comprised of the anomalous circulation of convergence and divergence zones in the east and west of Taiwan. It explained that the positive anomalous centres of precipitation in the Taiwan Strait were resulted indirectly from the unrealistic effect of the horizontal diffusion on the σ-surface. The above experimental results and detailed comparative analysis may lead to the conclusion that Scheme A not only directly brought about forecast anomalies in areas with steep mountain slopes

but also affected the surrounding areas via wavetrain propagation.

Ⅳ. CONCLUDING REMARKS

a. For the 4th order linear horizontal diffusion in a meso-scale model, calculation may be done on the σ-surface (0th order approximation)for variables u and v, or on the p-surface (1st order approximation) for variables T and q.

b. Scheme A may cause forecast anomalies, in and near areas of steep mountain slopes, including those of temperature, moisture, wind, precipitation, surface pressure as well as ground temperature, thus leading to forecast anomaly in surface flux.

c. The forecast anomalies above were due to Scheme A-predicted spurious increase of temperature at the lowest model level and moisture at the middle to lower levels near the mountain peaks, which yields, unrealistically, the thickening and strengthening of the unstable layer, the enhancement of convective development, and the increase of precipitation, as it gives opposite forecasts for mountain valleys. In addition, due to the convection anomaly in Experiment A, the lower-level convergence near the peaks and divergence near the valleys may enhance and bring about perturbation circulation that affects the surrounding areas via internal gravity wave propagation and thus lead to forecast anomalies.

d. Scheme B may be able to effectively suppress the forecast anomalies near steep orography, which may be initiated by the computational method on horizontal diffusion.

REFERENCES

Anthes R A, Eirh-Yu Hsie, Ying-hua Kou, 1987. Description of the PENN STATE/NCAR mesoscale model version 4 (MM4), NCAR technical note, NCAR/TN-XXX.

ECMWF, 1991 [Translation]. Data assimilation and medium range numerical weather prediction, Meteorological Press, 75—76 (translated & edited by the State Meteorological Centre of China).

Mellor G L, Blumberg, Alan F, 1985. Modeling vertical and horizontal diffusivities with the sigma coordinate system, *Mon. Wea. Rep.*, **113**: 1379—1382.

Smargrinsky J, 1963. General circulation experiment with the primitive equations, I : The basic experiment, *Mon. Wea. Rew.*, **91**: 99—114.

State Meteorological Administration of China, 1981. Typhoon Yearly Report 1980.

Taylor G I, 1954. The dispersion of matter in turbulent flow through a pipe, Proc., Roy., Soc., London, A223: 446—468.